JOURNAL OF MATERIALS SCIENCE 27 (1992) 3605–3616

Effects of ion implantation on the hardness and friction behaviour of soda–lime silica glass

S. J. BULL
AEA Industrial Technology, B 552, Harwell Laboratory, Didcot, Oxfordshire OX11 ORA, UK
T. F. PAGE
Materials Division, Department of Mechanical, Materials and Manufacturing Engineering, Herschel Building, The University, Newcastle-upon-Tyne NE1 7RU, UK

Ion implantation-induced changes in the near-surface mechanical properties of soda–lime silica glass have been investigated by indentation and scratch testing and have been found to be more complicated than changes in the corresponding properties of crystalline ceramic materials. Argon, nitrogen, carbon and potassium ions were used with energies in the range 45–300 keV. Hardness and scratch friction tests were performed under ambient laboratory conditions. At low doses, a decrease in hardness and an increase in both friction and surface stress are observed which are attributed to the electronic damage produced by ion implantation. At higher doses, the hardness increases again and a maximum is produced similar to the behaviour observed for crystalline materials. Similarly there is found to be a second stress and friction peak at this dose. This behaviour is shown to be due to the build-up of displacement damage produced by ion implantation and is thus very similar to the radiation hardening (and eventual amorphization) behaviour of ion-implanted crystalline ceramics. For glass, "amorphization" probably corresponds to some change in the existing amorphous state which, in turn, is responsible for the reduction in hardness, stress and friction at the highest doses.

1. Introduction

Ion implantation is a surface engineering technique whereby the physical, chemical and mechanical properties of the surface and near-surface region (< 200 nm depth) of a material can be controllably altered [1–3]. There have now been a considerable number of investigations of the mechanical and tribological properties of ion-implanted metals [4–6] and ceramics [7–12] but, by contrast, relatively little work has been reported on the effects of ion implantation on glasses. However, such previous observations [13–16] of the hardness response of implanted fused silica and soda–lime glass indicated that mechanical behaviour changes similar to those produced in crystalline materials may be induced by ion implantation. Both hardening and the reduction of the length of radial cracks around Vickers hardness indentations have been observed. However, no systematic study of the changes in tribological properties has been undertaken, and there is a considerable variation in observed properties between, for instance, fused silica and soda–lime glass.

In order to study further and clarify these issues, soda–lime glass has been implanted with a range of ions, at a range of energies, over a dose range from 1×10^{13}–5×10^{17} ions cm^{-2}. Ion species have been chosen which can become incorporated into the glass structure to varying extents. However, because of the already amorphous structure of glasses, experimental evidence for the changes in surface microstructure produced by ion implantation is less easy to obtain than for crystalline materials where implantation above some critical energy density renders the structure amorphous. However, the detailed structure of glasses is very sensitive to the linkage of co-ordination polyhedra and bonding. Thus, comparisons between the changing behaviour of ion-implanted glasses and similar changes in crystalline materials may give some clues as to the origins of implantation-induced modifications to the glasses.

2. Important damage mechanisms in ion implantation

As an implanted ion comes to rest in the surface of a material it loses energy in two ways. Inelastic collisions occurring at high energies lead to electronic damage in the target whereas elastic momentum-transfer collisions at lower energies can knock atoms from their structural sites. Such a displaced atom may have enough energy to cause further displacements and this leads to the formation of a displacement spike. Ultimately very low energy collisions lead to target heating before the implanted ion comes to rest. Such mechanisms apply equally well to glasses as well

0022–2461

as crystalline materials though the concept of a structural site is not so well defined. Suffice to say there is considerable structural reorganization within the displacement spike which might be expected to cause significant structural changes in the glass and thus give similar changes in mechanical properties to those observed in the implantation of crystalline ceramics. However, the electronic damage caused by the implantation process can also lead to changes in the bonding and local structural chemistry within glass structures and this will have to be taken into consideration if the mechanical properties of implanted glasses are to be fully understood.

Thus the interplay between energy deposited in displacement collisions and the energy deposited in electronic damage is important because this will affect the defects produced by ion implantation [14]. For a dose ϕ, the energy density deposited in nuclear collisions, E_{ND}, is given by

$$E_{ND} = \frac{E_c \phi}{4\Delta X_d} \quad (1)$$

where E_c is the energy deposited in nuclear damage processes per implanted ion (calculated by the method of Norgett *et al.* [17]) and ΔX_d the damage range deviation. This assumes that all of the nuclear damage energy deposition occurs within $2\Delta X_d$ on either side of the damage peak (see Fig. 1). Similarly, the electronic damage energy density is given by

$$E_{ED} = \frac{E_e \phi}{X_d} \quad (2)$$

where E_e is the energy deposited in electronic processes per incident ion (i.e. the difference $(E_0 - E_c)$ where E_0 is the ion-accelerating energy and E_c is the energy deposited in nuclear processes per ion as before), and X_d is the damage range. Because the electronic stopping cross-section is greater at high ion energies, it seems reasonable to assume that all the energy lost in electronic processes occurs before the nuclear damage reaches a maximum. X_d and ΔX_d can be calculated by a number of computer codes (e.g. EDEP-1 [18]).

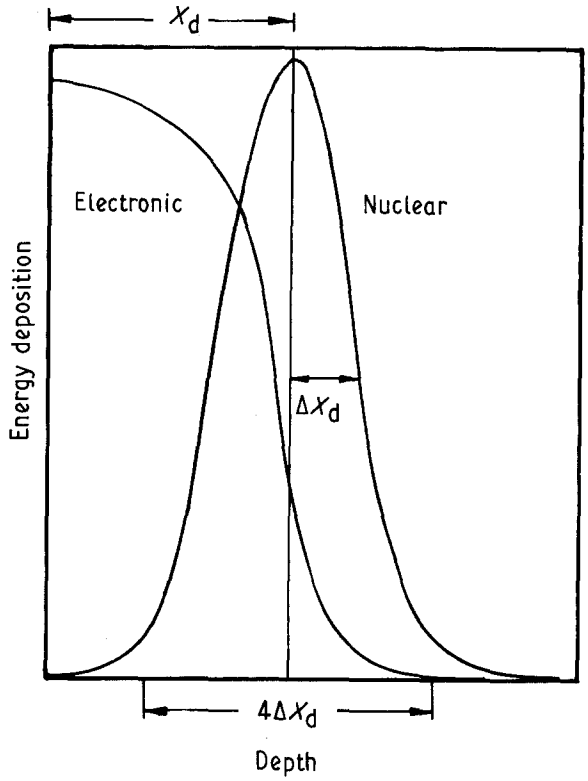

Figure 1 A schematic representation of the energy deposition with depth in materials implanted at intermediate energies ($\approx$ 100 keV). The majority of the electronic damage occurs closer to the surface than the nuclear/displacement damage. X_d is the damage range and ΔX_d its deviation. For the purpose of calculation, it is assumed that virtually all the nuclear (i.e. displacement) damage lies within $\pm 2\Delta X_d$ of the damage maximum.

3. Experimental procedure

Glass microscope slides of composition 22% Na_2O, 10.6% CaO, 5.4% MgO, 1% Al_2O_3, balance SiO_2 (all in at %) were cut into 25 mm × 20 mm × 2 mm sections, ultrasonically cleaned and degreased prior to implantation. The samples were then implanted with a range of ions in the Cockcroft–Walton facility at UKAEA Harwell. All implantations were performed at room temperature with a beam current of a few $\mu A\,cm^{-2}$ to doses in the range 10^{13}–5×10^{17} ions cm^{-2}. Implantation conditions and the range and damage parameters of the implanted ions (calculated using a modified version of the EDEP-1 computer code [18]) are given in Table I. The ion species were chosen to explore the behaviour of an inert gas virtually insoluble in glass (argon), a gas of higher solubility (nitrogen), a network modifying ion (potassium) and a potential substitutional ion (carbon) which might show a strong affinity for the silicon in the glass network. Energies were chosen to give comparable range of ~ 0.2 μm for each ion.

TABLE I Concentration and damage profile parameters (calculated by EDEP-1 [18])

Target	Ion	Energy (keV)	R_p (μm)	ΔR_p (μm)	X_d (μm)	ΔX_d (μm)
Glass	Ar	300	0.256[a]	0.067[a]	0.213[a]	0.077[a]
Glass	K	300	0.243	0.065	0.202	0.074
Glass	C	100	0.247	0.067	0.220	0.058
Glass	N[b]	90	0.203	0.060	0.181	0.054
Glass	N[b]	45	0.104	0.040	0.093	0.036

[a] R_p is the ion range and ΔR_p its deviation; X_d is the damage range and ΔX_d its deviation.
[b] A 90 keV nitrogen beam was used which contains 75% N_2^+ and 25% N^+ at this energy. The N_2^+ splits up to give two N^+ at 45 keV on hitting the substrate.

The mechanical properties of the implanted glasses were investigated using microhardness and scratch testing [1, 2]. All microhardness indentations were performed with a Leitz miniload 2 microhardness tester and were made under standard conditions (ambient temperature, humidity 50%–80%, laboratory air, 15 s dwell time). For hardness measurements five Knoop indentations were made on each sample at loads of 10 g and 25 g in order that the majority of any plastic zone associated with the indentation should lie in the implanted layer. For measuring changes in surface stress state, the changes in length of the radial cracks around a 500 g Vickers hardness impression as a function of implantation dose was investigated. Cracks ending close to the indentation or showing significant branching were ignored and enough indentations were made so as to obtain 20 crack measurements. For some of the high-dose implants this required a considerable number of indentations (> 100).

The change in crack length can be used to measure the surface stress state following the work of Lawn and Fuller [19]. The thickness of the damaged layer, d, was assumed to be $4\Delta X_d$ and the fracture toughness of the unimplanted material, K_c, was determined from indentation cracks using the formulation of Anstis *et al.* [20, 21]. Surface stresses were then calculated from the equation

$$1 - \left(\frac{C_0}{C}\right)^{3/2} = \frac{2S}{K_c d^{1/2}} \quad (3)$$

where C_0 is the crack length in unstressed material, C the crack length in the implanted specimen and S is the integrated stress.

Specimens were scratched in air under ambient conditions on a single-pass scratch rig at a sliding speed of 0.25 m s^{-1}. The scratch tester is described in more detail elsewhere [2]. A 220 μm spherical-tipped diamond stylus was used for all the tests which was run in an unimplanted material prior to testing. All the implanted flats were carefully cleaned and degreased in alcohol prior to testing.

One problem which was observed during the course of this study was the tendency of the samples implanted with gaseous ions to lose some of the gas over a period of time after implantation. This resulted in changes to the measured properties with time for both the argon and nitrogen implants which were not observed for the carbon and potassium implants. In order to reduce this effect, measurements were made as soon as possible after implantation on all the samples investigated here. Measurements made over a period of 2 years after implantation on the argon-implanted specimens showed that the magnitude of the hardness changes was reduced and the implantation-induced stresses were also almost totally removed. The performance of components implanted with inert gases are also expected to change with time and this will be unacceptable in most applications. It is thus vitally important to check that the structure composition of the implanted layer does not change during testing if the results are to be free from such errors.

4. Results and discussion

4.1. Microhardness

Figure 2 shows the microhardness behaviour of these materials. All the implanted glasses show a distinct drop in hardness at low doses ($\approx 5 \times 10^{14}$ ions cm^{-2}), followed by a hardness peak at higher doses ($\approx 10^{16}$ ions cm^{-2}) and a softening at the highest doses. This latter peak, followed by softening, is very similar in both form and energy deposition/dose to the peak in hardness associated with radiation damage, followed by softening, associated with amorphization in crystalline ceramic materials. This suggests that some damage-induced structural change is occurring, similar to the amorphization process in crystalline materials. This "amorphization" of the glass specimen is more difficult to understand because the material itself is initially amorphous. However, the accumulation of both implanted atoms and damage in the implanted layer will result in an amorphous layer with a substantially different structure and properties to the unimplanted glass. The transition will probably involve significant structural rearrangement and possible incorporation of the implanted ions into the glass network. Accompanying implantation there is an expansion of the implanted layer, the extent of which depends on the implanted dose (typically < 100 nm). This can be determined from surface profilometer traces across the boundary of the implanted region. Once amorphization has occurred there is a much more rapid expansion of the surface layer and the steps become larger but the size of the expansion depends on the implanted ion (typically > 100 nm). The inert gas argon and to a lesser extent the nitrogen implants lead to much greater expansions than the other ions. Although the expansion of the surface implies a reduction in density within the implanted region, the scatter in the measured values makes it very difficult to draw any firm conclusions about this.

For the argon implanted glass the amorphization phenomenon is accompanied by a very rapid drop in surface hardness, which is very different from the behaviour observed for the other implanted glasses. This rapid softening is due to the formation of a layer of argon bubbles below the surface as is discussed in Section 4.3. These bubbles probably contribute to the rapid expansion of the amorphous layer with dose observed for argon-implanted glass. Bubble formation was also observed (but to a much lesser extent) in the case of nitrogen-implanted glass but in this case the dose required to produce bubbles was very much higher ($> 5 \times 10^{17}$ N_2^+ cm^{-2}). This would imply that nitrogen shows a higher solubility in the glass than argon and may become incorporated into the glass network. Blistering in high-dose nitrogen-implanted glass has been observed previously [22].

From the dose at which softening occurs (i.e. $\sim 5 \times 10^{16}$ Ar^+ cm^{-2} for argon-implanted soda–lime glass) the critical energy density for amorphization (CECA) can be calculated for this material [7]. This value is 4×10^{22} keV cm^{-3} which is about 500 eV per atom of the target. For predominantly covalent materials such as silicon the amorphization energy is about 1×10^{21} keV cm^{-3} (20 eV/atom) at room tem-

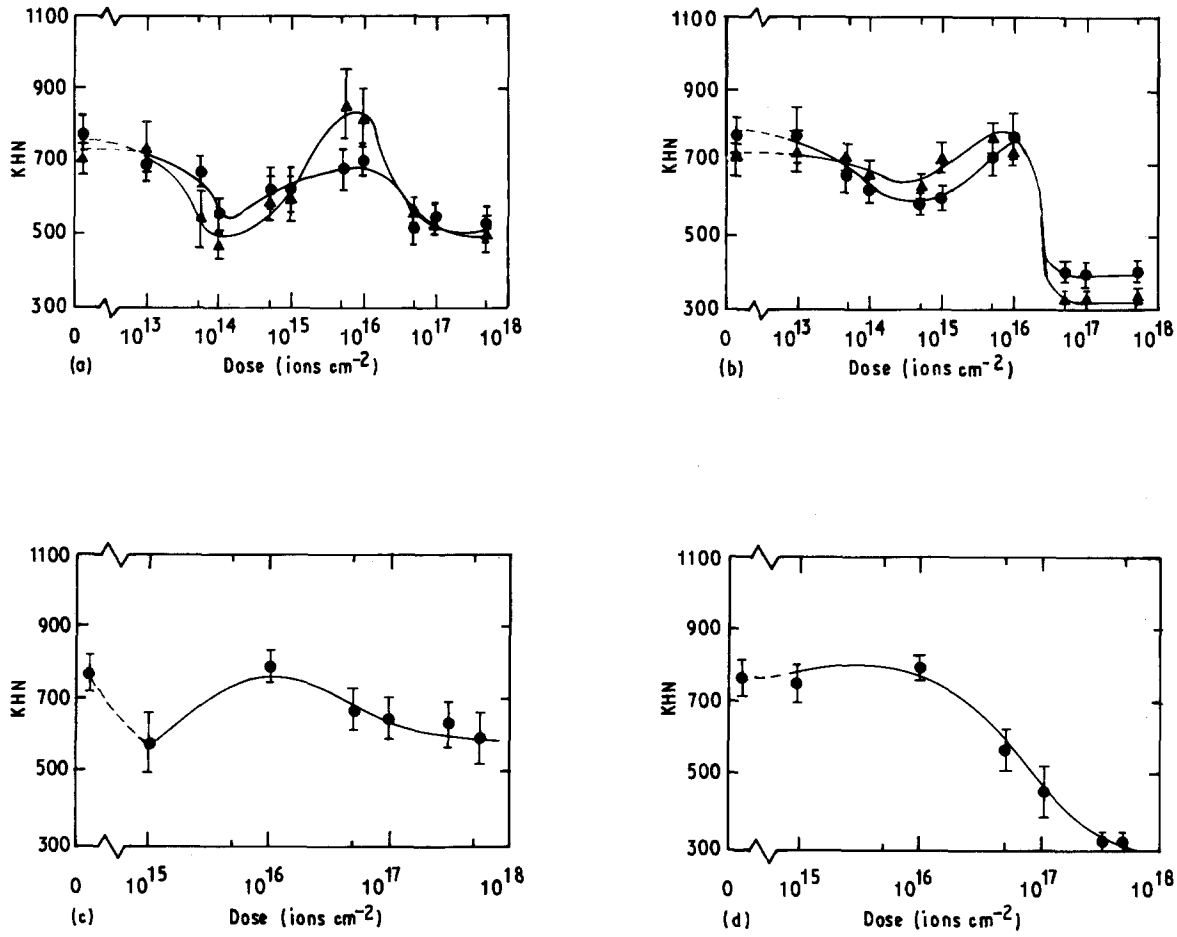

Figure 2 Variation of Knoop microhardness with dose for soda–lime–silica glass implanted with (a) 300 keV K^+, (b) 300 keV Ar^+ (c) 100 keV C^+ and (d) 90 keV N_2^+. In all cases the hardness initially decreases before rising to a maximum at higher doses. This high dose maximum is similar to the behaviour for crystalline ceramics and the reduction in hardness above this dose is attributed to a similar "amorphization" phenomenon. (▲) 10 g, (●) 25 g.

perature, whereas for predominantly ionic materials the CECA is $\sim 6 \times 10^{23}$ keV cm^{-3} (5080 eV/atom). Soda–lime glass consists of a covalently bonded Si–O tetrahedral network with about 10% ionic bridges of the form

$$\begin{array}{c} | \quad Na^+ \quad | \\ -Si-O^- \quad {}^-O-Si- \\ | \quad Na^+ \quad | \end{array}$$

In the absence of any better model, it might be assumed that the overall amorphization energy could be taken as the sum of the amorphization energies for the covalent and ionic parts of the glass. In this case the CECA for glass is given by $0.9 \times 20 + 0.1 \times 5080 = 526$ eV/atom. This is very close to the estimated value for glass ($\sim$ 500 eV) and it thus seems likely that the softening is associated with the "amorphization" process. A better model would be to identify the critical bonding changes necessary to allow the various co-ordination polyhedra to gain sufficient flexibility to reorganize themselves into a new structure but we know of no satisfactory way of doing this.

The drop in hardness at low doses cannot be attributed to such displacement damage. However, Mazzoldi and co-workers (e.g. [23–26]) have reported that implantation of soda–lime glass with heavy ions results in the depletion of network-modifying sodium in the implanted layer. The charged implanted ions free the sodium from the network which then diffuses out of the implanted layer reducing the network strength of the glass there. According to the result of Battaglin *et al.* [15] the same depletion occurs for any alkali modifier. The alkali is removed by preferential sputtering at the surface of the glass during implantation. This preferential sputtering sets up a concentration gradient and the released alkali migrates towards the surface under this driving force. The process is greatly enhanced by radiation-enhanced diffusion which will be promoted by the defects created by nuclear energy deposition.

A mechanism by which the sodium is released has been proposed by McCaughan *et al.* [27]. Ions with a high ionization potential such as Ar^+ have a high neutralization probability when approaching a surface to within a few tenths of a nanometre. In an insulator the ion is neutralized by an electron originating from the outermost monolayers of the surface and the ion thus travels into the bulk as a neutral atom. In this process a positive hole is created, the most probable reaction being

$$\equiv S\text{–}O\text{–}Na + Ar^+ \rightarrow \equiv Si\text{–}O + Na^+ + Ar \quad (4)$$

where the sodium ion is no longer bonded to the non-bridging oxygen atom and can move into the bulk.

Smetts and Lommen [28] report XPS evidence for the formation of the trapped holes (≡SiO groups) in which the oxygen atoms bear no formal charge. (According to Smetts and Lommen [28], the removal of an electron from the surface of the glass to neutralize the incident argon ion leaves a positive hole where the sodium ion is no longer bonded to the non-bridging oxygen atom. The fate of the Si≡O groups is less well understood but it is probable that they combine to form –Si–O–Si– bridges with the evolution of oxygen.)

However, Burrow *et al.* [29] report that sodium depletion also occurred for potassium implants in sodium trisilicate glass and thus the mechanism for sodium release may not be as simple as the McCaughan *et al.* model. What is certain is that the release of sodium occurs because of an electronic interaction between the modifying sodium and the implanted ion, and thus the process will depend on the electronic energy deposition.

In unimplanted modified glasses, deformation would be expected to follow planes with a high density of network modifiers. In the implanted glasses the removal of the modifying ions would make such a deformation easier and thus lower the microhardness of the material. For all ions a similar softening to that observed for argon-implantation was produced, demonstrating the importance of structural disruption in softening. At intermediate doses, the effects of radiation hardening begin to dominate and the hardness increases again up to the hardness peak prior to softening on "amorphization" described earlier. The radiation-hardened material is only ever as hard as the original unimplanted samples. Thus it would appear that some ≡SiO groups recombine to form new bonds, probably ≡Si–O–Si≡, and this process requires displacement damage to cause sufficient disruption within the glass network. Indeed, Smetts and Lommen [28] report that there is evidence for the formation of Si–O–Si bridges from the ≡SiO groups with the release of oxygen. Thus some hardening can occur even in situations where the implanted ion cannot be incorporated into the network (e.g. for argon implantation). However, the radiation hardening is more pronounced for the potassium implant indicating that some bridges have been recreated incorporating these modifying implanted ions.

Thus it can be seen that two distinct regions of hardness change occur for ion-implanted soda–lime glass. At low doses there is a softening associated with the release of sodium from the glass network. At higher doses, hardening presumed due to radiation damage-controlled mechanisms begins to dominate until sufficient damage is accumulated for "amorphization" to occur when there is some softening. This behaviour will have implications for the implantation-induced stresses.

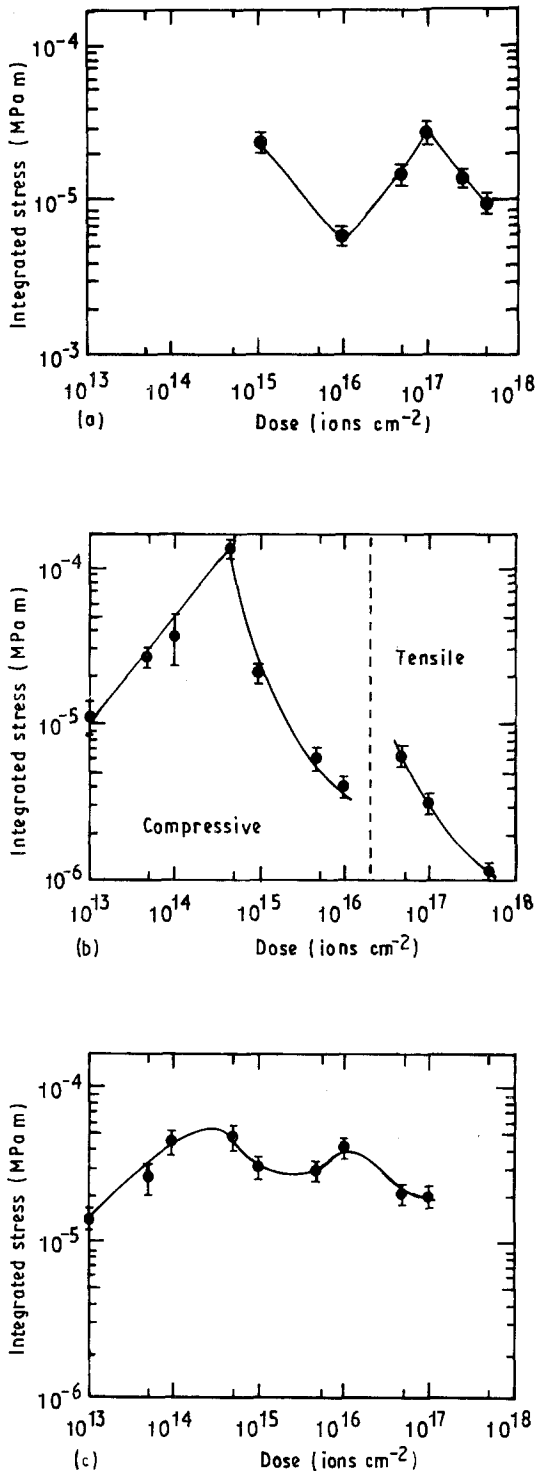

Figure 3 Plots of integrated stress (as determined by the indentation fracture method using 500 and 100 g Vickers indents) against dose for (a) 100 keV C^+, (b) 300 keV K^+ and (c) 300 keV Ar^+ implanted soda–lime–silica glass. Two stress peaks are produced in this material. In (b) the second peak is complicated by the change in sign of the stress resulting in there being a tensile maximum at a dose of 3×10^{16} K^+ cm^{-2} with the tensile stress then decreasing at higher doses.

4.2. Implantation-induced stresses

The surface stress variation for soda–lime glass is somewhat more complicated than for crystalline materials (Fig. 3). Two distinct peaks are visible; for the argon implants both peaks are compressive whilst for the potassium implant the first peak is compressive and the second peak tensile. This is a distinct contrast to the single peak corresponding to amorphization of crystalline ceramics. For the glass implants, the second peak corresponds to the dose for "amorphization" reported in the previous section whilst the first peak is at a considerably lower dose.

Fig. 4 shows the integrated stress plotted against the energy deposited in nuclear processes and electronic processes for our 300 kV Ar^+ results and integrated stresses calculated from the 500 g crack-length data of Battaglin *et al.* [15]. From Fig. 4a it can be seen that there is a reasonable correspondence between the energy densities of the high dose stress peaks at around 4×10^{22} keV cm^{-3}, whereas the correspondence between the positions of the lower dose stress peak is not so good. Thus the second stress peak is due to the damage caused by displacement processes, which is the origin of the single stress peak in crystalline materials. From the plot of integrated stress against electronic damage energy density (Fig. 4b), it can be seen that the first stress peaks now show reasonable correspondence at an energy density of 3×10^{21} keV cm^{-3}. Thus the initial stress peak seems to be due to the damage caused by electronic processes, i.e. the processes responsible for the freeing of the sodium network modifiers and reducing the hardness of the implanted layer described in the previous section. The first stress maximum is thus produced at doses where displacement damage begins to be significant and allows structural relaxation of the stress progressively being built up by electronic damage. As the dose is further increased the volume expansion accompanying increasing displacement damage leads to a second increase in stress. The second peak is created by stress relaxation on "amorphization".

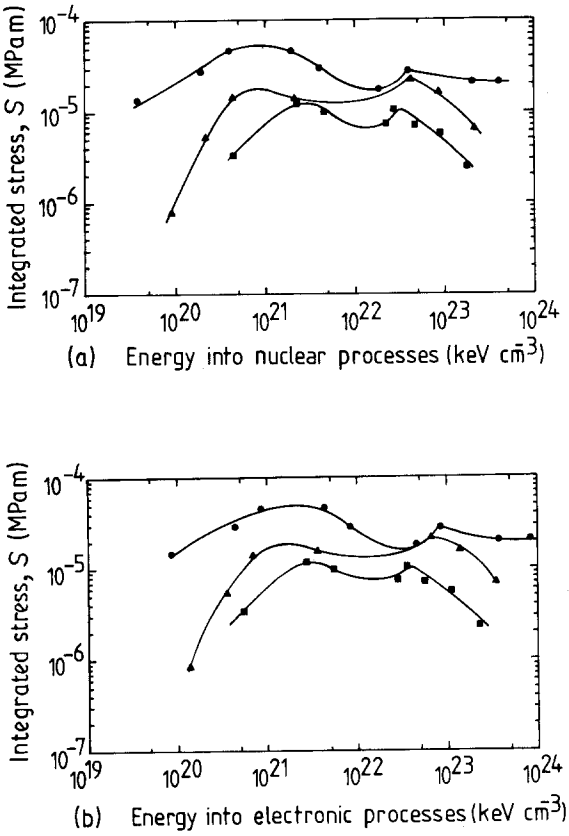

Figure 4 Plots of the variation of integrated stress with (a) energy deposited in nuclear processes, (b) energy deposited in electronic processes for soda–lime glass, implanted with argon over a range of energies. Of the two stress peaks, the coincidence of the lower dose peaks is better on the electronic damage plot while the higher dose peaks coincide better when plotted against nuclear damage. The error bars have been removed for clarity but are typified by those of Fig. 3c which shows the same 300 keV results. (■) 50 keV, (▲) 100 keV, (●) 300 keV.

The fact that two distinct stress peaks form in this material is indicative of the fact that at least two stress-relieving mechanisms must occur during implantation. By contrast, Eernisse [30] showed that a single tensile stress peak was formed for the implantation of fused silica, but this was produced by two different compaction mechanisms (one as a result of electronic damage and the other as a result of displacement damage). Double peaks, similar to those found here, have been observed for borosilicate glasses [31], with both tensile and compressive stress peaks formed as with the potassium implanted case here. This was attributed to the alkali being in two different sites in the glass network, with different binding strengths. The mechanisms for alkali release and hence stress generation were thought to be entirely due to electronic damage. The electronic energy deposition levels in the present study are much higher than those used by Arnold [31] and thus it seems likely that the reason for the two stress peaks formed is different from this.

The detailed mechanism for the stress relief in the soda–lime glass that is responsible for the creation of the second stress peak is as yet unknown, but is expected to be a function of the displacement damage produced by the implanted ions. As such it should be independent of the ion species used, but the results for the potassium implant look very different at first sight. Here the second stress peak is tensile rather than compressive. Because potassium is a larger ion than sodium, it might be expected that replacement of the sodium with potassium would result in compressive stresses in the surface layer. Indeed ion-exchange experiments [32] show that replacing sodium with potassium can lead to a maximum compressive integrated stress in the surface layer of 3.3×10^{-6} MPa m which is much smaller than the implantation-induced stresses observed in this study.

Tensile stresses have been reported for potassium-ion-exchanged glasses [33] where the ion-exchange process was carried out close to the softening temperature of the glass. In this case the tensile stresses were attributed to thermal expansion mismatch between the ion-exchanged surface layer and the bulk. The thermal expansion coefficient of glasses modified with potassium is larger than that of identical glasses modified with sodium over the complete composition range [34] and thus in cooling down from the ion-exchange temperature it will produce a larger contraction in the ion-exchanger layer than in the bulk. Hence tensile stresses are generated. In fact, the thermal expansion coefficients of mixed alkali glasses with varying Na/K ratios were found to be larger than predicted by a simple method of mixtures [34] and thus the tensile stress generation will be even more pronounced. In order that these tensile stresses exceed the compressive ion-exchange stresses, some stress relaxation must have taken place at the ion-exchange temperature.

For the specimens implanted in this study, a similar process may be taking place. The displacement damage produced by ion implantation causes some structural relaxation at doses around 5×10^{14} ions cm^{-2} (as

shown by the reduction in the integrated stresses in argon-implanted glass above this dose) and this structural rearrangement may be sufficient to allow the thermal expansion stresses to affect the final stress state of the material. The temperature rise during implantation for this specimen is estimated to be about 150 °C at a dose of 5×10^{14} K^+cm^{-2}. After implantation, in cooling down from this temperature, the compressive implantation-induced stresses are reduced by the tensile thermal expansion mismatch stresses. The surface stresses are tensile by a dose of 5×10^{16} K^+cm^{-2}. The decreasing tensile stress at high doses is thus due to the increasing compressive stresses produced by the nuclear displacement damage which is responsible for the second stress peak in the case of argon implantation.

As discussed above for fused silica, the generation of stress has been attributed to the radiation-induced compaction of the glass structure. The density of modified glasses is larger than that of fused silica so it is unlikely that this mechanism will be important in soda–lime glass. RBS observations of potassium implanted sodium trisilicate glass by Burrow *et al.* [29] show that the integrated area of the potassium implant peak is substantially lower than the implant ion density impinging on the target. Also a substantial surface potassium peak was observed. A migration of 30%–40% of the implanted ion towards the surface had occurred where it can be lost by preferential sputtering in a similar manner to the sodium. The compressive stresses due to electronic damage generated by potassium implantation are larger than those generated by argon implantation. It thus seems that the removal of native potassium from the material at low argon doses has resulted in a large volume expansion and reduced bond formation in the implanted layer. In this situation some compaction of the implanted layer may occur and tensile stresses may be generated. However, whether the compaction is due to structural relaxation or ion bombardment is unknown.

4.3. Bubble formation in argon-implanted glass

As mentioned in Section 4.1 the "amorphization" phenomenon is accompanied by a very rapid drop in surface hardness which is very different from the behaviour observed for the other implanted materials. Reflected-light microscopy of specimens implanted to 1×10^{17} Ar^+ cm^{-2} shows that a number of bubbles have formed in the surface layer (Fig. 5). In specimens implanted to 5×10^{16} Ar^+ cm^{-2} the surface layers around indentations can be removed during the indentation process (Fig. 6a). Such areas have been analysed by EDX in the SEM and both the removed material and the uncovered surface contain a small amount of argon compared with a general area of the surface which has not been removed. Thus it seems likely that these bubbles contain argon rather than oxygen released from the target.

The bubbles can be clearly seen in TEM specimens made from the exfoliated surface material in 5×10^{16} Ar^+ cm^{-2} implanted sapphire. The bubbles are faceted which implies that the argon inside them is crystalline (or the glass surrounding the bubble has crystallized). The fact that the bubbles appear darker than the surrounding glass (i.e. the electron density in the bubble is higher than the glass) implies that the argon is indeed under high pressure. Similar results have been reported for helium bubble-implanted metals [35], and for higher atomic number gases, such as krypton, in aluminium [36].

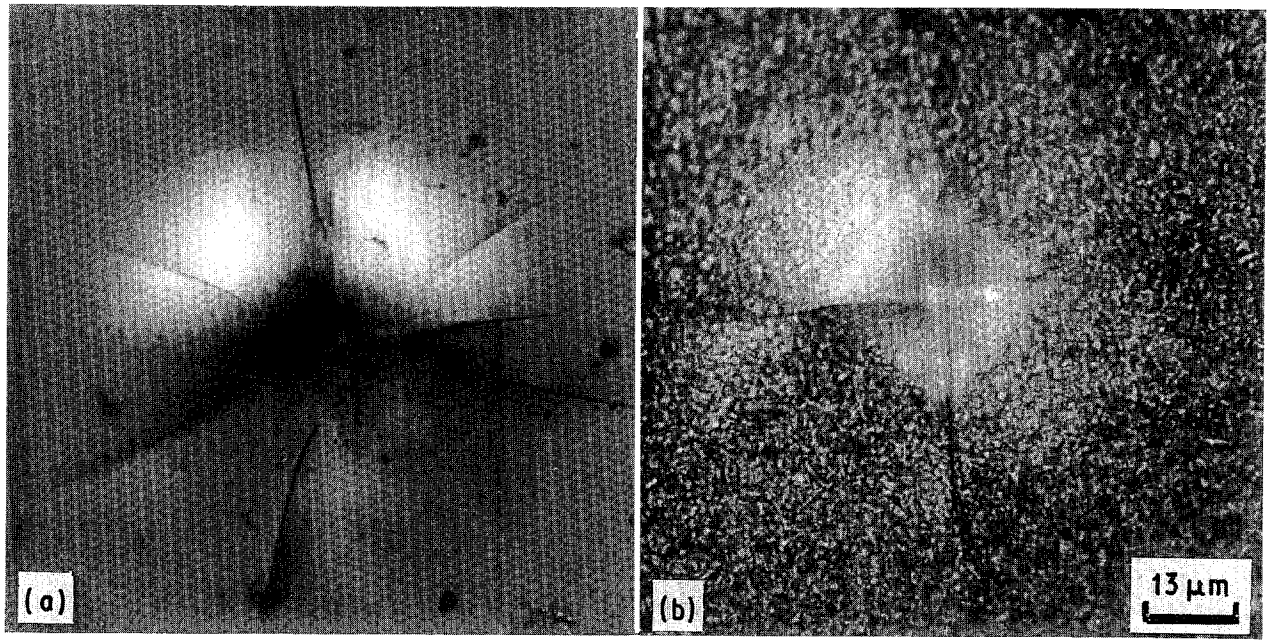

Figure 5 Reflected-light micrograph of a 500 g Vickers indentation in (a) 1×10^{17} Ar^+ cm^{-2} and (b) 5×10^{17} Ar^+ cm^{-2} implanted soda–lime glass. Visible bubbles can be seen in the lower dose-implanted specimen. As the dose is increased, the amount of bubble formation also increases, until by 5×10^{17} Ar^+ cm^{-2} the surface is heavily blistered due to the breaking open of surface bubbles.

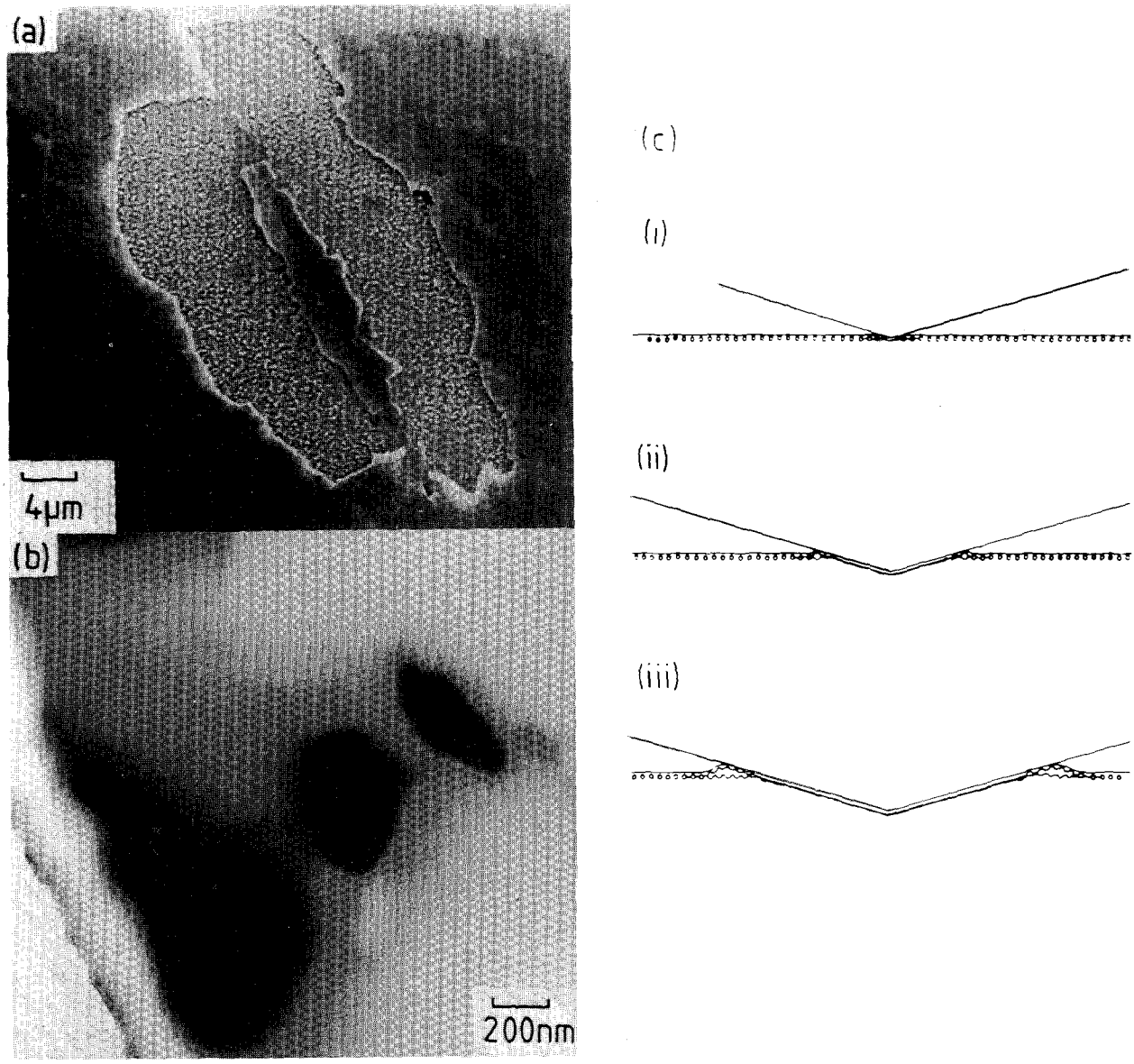

Figure 6 (a) A secondary electron SEM image of a 25 g Knoop microhardness indentation in 5×10^{16} cm^{-2} Ar^+-implanted glass. A region of material around the indentation has been exfoliated due to the presence of a subsurface argon bubble layer. (b) TEM (100 kV) micrograph of some of the exfoliated material, showing these argon bubbles. The bubbles are darker than the surrounding glass indicating that there is a higher electron density within the bubble than around it. *In situ* EDX analysis reveals predominantly argon in these areas. (c) Schematic diagram of the generation of exfoliated material: (i) bubbles are compressed and connected by fracture parallel to the surface; (ii) the bubbles are compressed flat forcing argon to the edge of the contact area; (iii) the accumulation of argon at the edge of the contact area causes lifting and bending of the material around the indentation, which may fracture and become removed to form the exfoliated material. Because the surface layer is no longer completely attached to the substrate in the indented area, this may be removed on unloading by adhesion to the indenter.

EDX analysis in the regions between bubbles in the higher dose implants reveals that there is very little argon dissolved in the surface layer once the bubbles have formed. The size of the bubbles increases with dose. Table II shows the mean bubble radius, r, and the mean bubble separation for all doses where the bubbles could be seen either by light microscopy or in the SEM. The pressure of gas in the bubbles may be calculated from its radius by

$$P = \frac{2\gamma}{r} \quad (5)$$

where γ is the surface energy of the bubble. It is likely that the surface energy will be altered by implantation, but because argon is almost insoluble in glass the change will be small. Thus the bubble pressure may be estimated using the surface energy of unimplanted soda–lime glass ($\gamma = 0.5$ J m^{-2} [37]) and calculated values are given in Table II.

TABLE II Bubble parameters in argon-implanted glass

Dose (ions cm^{-2})	Mean radius, r (μm)	Mean separation (μm)	Mean pressure (MPa)
5×10^{16}	0.3	0.7	3.3
1×10^{17}	0.5	1.0	1.0
5×10^{17}	1.0	1.3	1.0

The sizes of the bubbles seen here are of the same order as the widths of the concentration or damage peaks (taken as $4\Delta R_p$ or $4\Delta X_d$, respectively). It may be that the bubbles are confined to the highest damage

regions and thus have a flatter shape than assumed. There is some evidence from this transmission electron micrographs taken at $\sim 30°$ tilt where some shortening of the bubbles was observed. However, the degradation of the image due to the increased specimen thickness that the electron beam has to pass through at high tilt angles, makes it difficult to make confident estimates of the bubble thickness (see Fig. 7).

At the doses where bubble formation has just occurred, the bubbles layer is nearly continuous, because the bubble separation is nearly the same as the bubble radius. For higher doses (e.g. 1×10^{17} Ar^+ cm^{-2}) the bubbles are larger and occupy a larger volume fraction due to their increased argon content and lower pressure [38].

On loading an indentor on to the surface of an implanted specimen, the bubbles are put into compression. The gas pressure inside even the smallest bubbles (3.3 MPa) will be small compared with the indentation pressure of ~ 7 GPa (typical hardness of glass). The gas pressure in the bubbles is expected to rise as the bubbles are compressed (assuming the argon does not redissolve) and flattened to a more pronounced disc-like geometry. This is expected to provide the driving force for the sideways linkage of bubbles to take the configuration of cracks parallel to the surface. The gas is forced out to the edge of the contact area, thus detaching the surface layer from the bulk. The indentation is surrounded by a halo of removed material. This exfoliation of surface material renders the indentation diagonals impossible to measure accurately and the tendency is to overestimate, resulting in substantially lower hardnesses.

For higher doses the bubbles are easily compressed because of the lower bubble pressure. Also the inter-bubble separation is larger and the compressing of a single bubble will have little effect on the surrounding bubbles. In this case the implanted layer's deformation properties will be more similar to a spongy material. The reduced energy expended in compacting the bubbles leaves more available for the formation of the indentation and thus the material appears much softer. At the very highest doses (5×10^{17} Ar^+ cm^{-2}) the bubble layer extends to the surface and blistering is observed.

Thus it can be seen that the argon bubbles form at doses above $\sim 5 \times 10^{16}$ ions cm^{-2}. The presence of bubbles in the surface layer results in a reduction in surface hardness and exfoliation around hardness indentations. Such behaviour has also been observed for inert gas implantation in sapphire [39] and is probably a function of the insolubility of argon rather than any target properties.

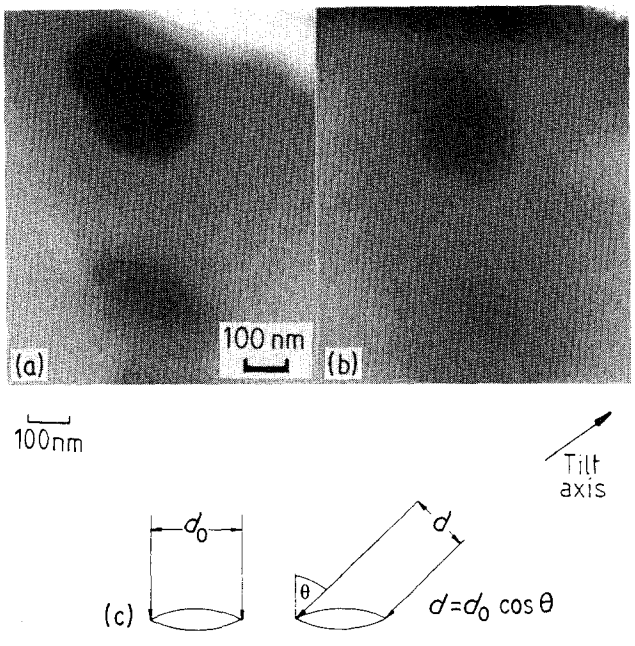

Figure 7 Transmission electron micrographs of bubbles in 5×10^{16} Ar^+ cm^{-2} implanted glass (a) with the electron beam normal to the implanted surface, (b) with the electron beam at 30° to the implanted surface. The bubbles in (b) are foreshortened, indicating that they are not spherical, but may be lenticular in shape (c).

4.4. Friction

Bowden and Tabor [40] suggests that the friction force, F, can be separated into a component due to adhesion (or shear within the softer material [41]) and another due to ploughing, namely

$$F = A_1\tau + A_2P' \quad (6)$$

where A_1 is the real contact area, A_2 is the cross-sectional area of the track produced, τ is the shear strength of the interface or the weaker of the two materials, and P' is the plastic flow stress of the material being ploughed (usually taken as its hardness). In most low-load scratch tests where the plastic deformation is confined to the implanted layer, the friction will be dominated by the shear/adhesion term.

The coefficient of sliding friction of diamond sliding against both implanted and unimplanted glasses is a very sensitive function of both the slider material, the environment and the load used. For the unimplanted glass investigated here Fig. 8a shows the variation of coefficients of friction with load, together with the ploughing coefficient of friction calculated from the measured track width using the method of Goddard and Willman [42] detailed elsewhere [41]. The friction at low loads is dominated by ploughing, but as the load is increased adhesion becomes dominant. At the loads where the plastic deformation associated with the scratch is mainly in the implanted layer, the friction is dominated by the plasticity of this surface layer and the friction should thus correlate well with the hardness changes reported in Section 4.1. The increasing dominance of the shear strength of the glass substrate as the load is increased is shown in the calculated shear strengths from the friction data in Fig. 8a which are presented in Fig. 8b.

The dose variation of the coefficient of friction, μ, is shown in Fig. 9. For all the curves presented there are two peaks in friction, one at a relatively low dose around 10^{15} ions cm^{-2} and another at the higher dose of 10^{16} ions cm^{-2}. The latter peak corresponds to a peak in hardness as shown in Fig. 2 and thus this represents a change in surface plasticity. The low-dose peak corresponds to a hardness minimum, but a maximum in residual stress which was correlated with

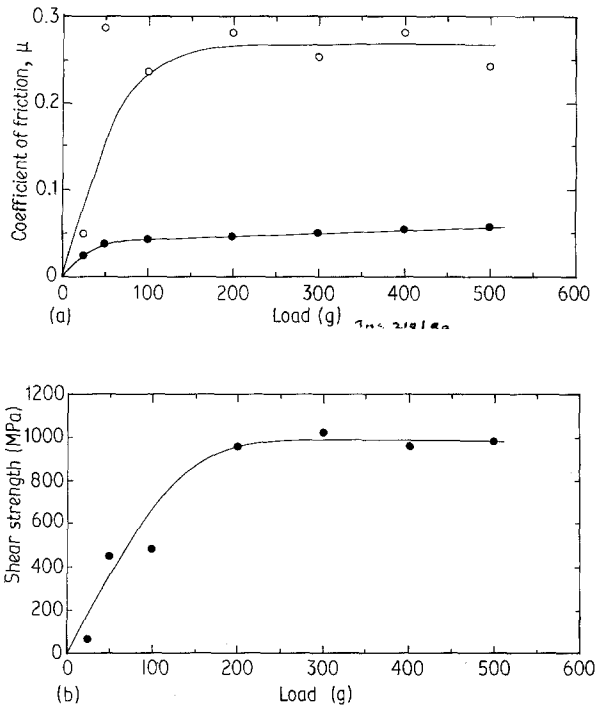

Figure 8 (a) Variation of coefficient of friction with normal load for unimplanted soda–lime glass. The measured (○) friction is shown compared with the calculated ploughing (●) friction (using the model of Goddard and Willman [42]) thus demonstrating a dominance of adhesive processes in the observed friction response. (b) Shear stress (controlling adhesion) calculated from the friction data in (a).

associated with electronic damage in Section 4.2. Thus it would seem that this peak is not due to changes in surface plasticity but due to changes in diamond/implanted glass adhesion. Because this low-dose peak was not observed in our previous investigations on these implanted specimens [2], this explanation would seem most likely. In the earlier studies, no attempt was made to control the humidity during the scratch test and the glass surfaces were probably heavily covered with surface adsorbates which led to chemomechanical softening of the surface layer as evinced by the much wider scratch tracks produced than observed in later experiments. In this case, the diamond penetrated deep into the glass surface and the changes due to ion implantation were lost within the substrate effects. Furthermore the presence of these adsorbates would be expected to reduce indenter/substrate adhesion and hence reduce the adhesion contribution to friction.

The scratch testing of the implanted glasses proved very difficult to perform reproducibly. The simple cleaning treatments that worked well for single sapphire [2] were much less successful for the glass substrates and for this reason it proved impossible to make reliable friction measurements using spheres to remove the effects of plasticity in the scratch test. Furthermore, because the glass substrates were transparent it proved very difficult to measure the track widths accurately by reflected-light microscopy (the scratches show virtually no contrast in the SEM) and for this reason no detailed analysis of the friction results has been attempted.

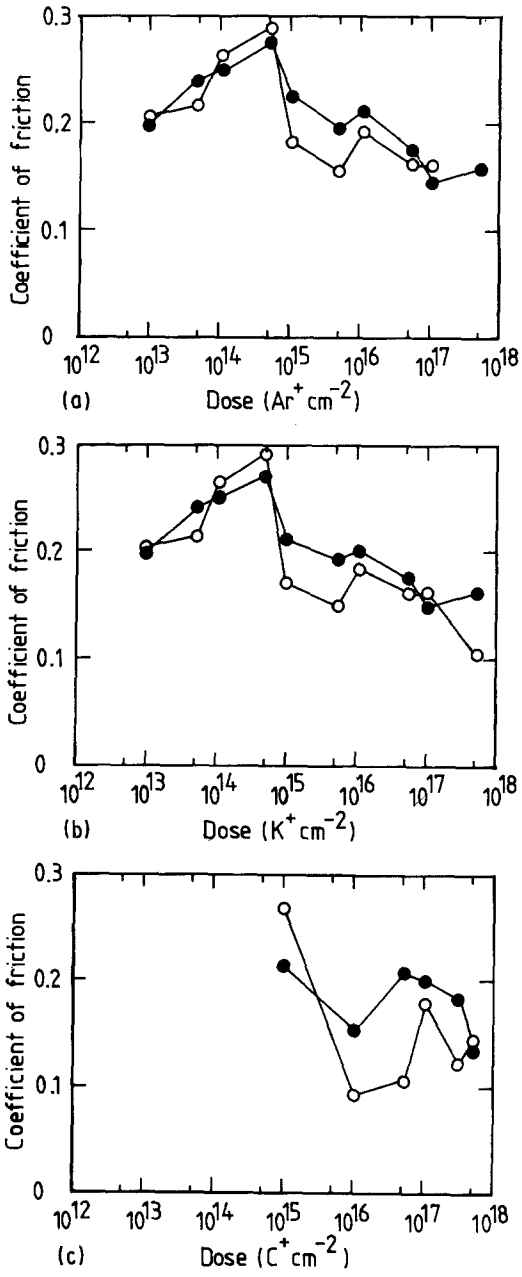

Figure 9 Plots of coefficient of friction against dose for soda–lime glass implanted with (a) 300 keV Ar^+, (b) 300 keV K^+ and (c) 100 keV C^{4+}. (○) 25 g, (●) 50 g.

5. Conclusion

The changes in the near-surface mechanical properties of ion-implanted glasses are more complicated than those of crystalline ceramics and, due to their amorphous nature, it is difficult to investigate the nature of the implantation-induced changes in surface microstructure responsible for these properties. The properties measured in this study have been found to be dependent on the time that has passed since implantation and this must be borne in mind when making comparisons between materials implanted at different times.

The microhardness of an implanted soda–lime–silica glass was found to decrease at low doses and increase again at higher doses up to a maximum. This high dose reduction in hardness was attributed to an "amorphization" phenomenon similar to that observed for crystalline materials. The implantation-induced stresses increase at the low doses where the

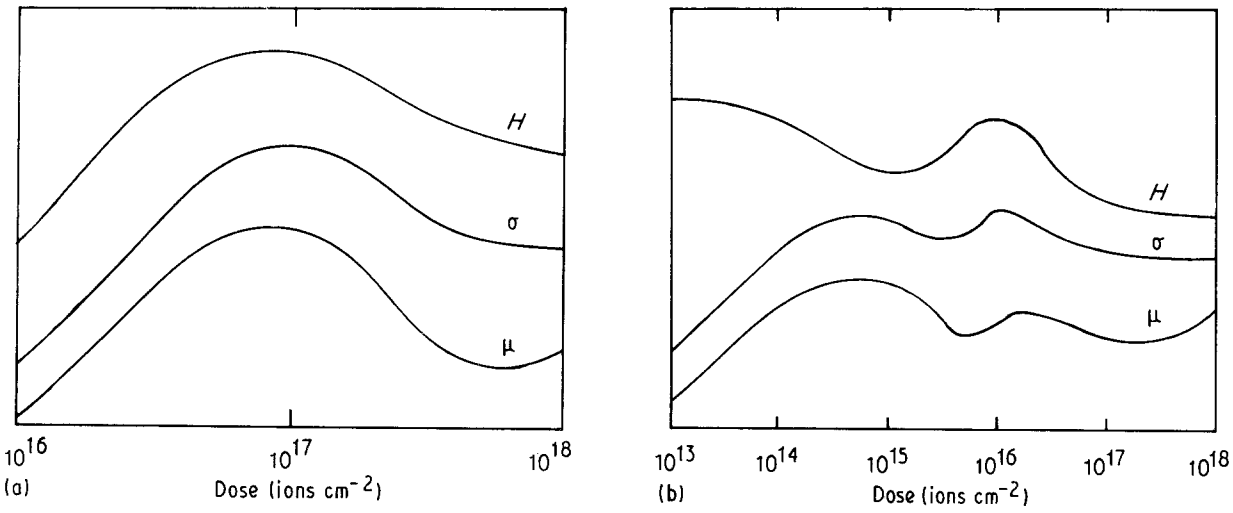

Figure 10 Schematic variation of the hardness, H, surface stress, σ, and coefficient of friction, μ, with dose for (a) titanium-implanted sapphire and (b) argon-implanted glass. The single peak in these properties at the onset of amorphization in crystalline materials is contrasted with the more complicated twin-peak behaviour of the glasses.

hardness is reduced, and decrease again as the hardness begins to increase. A second stress peak is formed at the higher doses where the hardness maximum occurs. There are thus two distinct regions of behaviour which have been attributed to different damage processes occurring during implantation. The low-dose behaviour is expected to have its origin in electronic damage, whereas the high-dose behaviour has its origin in displacement damage. Thus the high-dose behaviour is similar to that in crystalline materials. The variation of coefficient of friction with dose also shows two peaks, the lower dose of which can be attributed to the same electronic damage mechanism. The form of the electronic damage is as yet unknown, though the property changes are thought to be due to the freeing of the network modifying sodium from the glass by the implanted ions.

In conclusion, it can be seen that at high-dose ion-implanted glasses behave in an identical manner to implanted ceramics, whilst at lower doses the electronic damage may be significant and other effects will occur. Fig. 10 shows a schematic comparison of the behaviour of crystalline materials and glasses with ion-implantation dose. The precise balance of properties will thus depend on the nature of the substrate, together with the ion/energy/dose combination used.

Acknowledgement

The authors thank Dr G. Dearnaley, Harwell, for provision of the implanted samples.

References

1. P. J. BURNETT and T. F. PAGE, *J. Mater. Sci.* **19** (1984) 3524.
2. S. J. BULL and T. F. PAGE, *ibid.* **23** (1988) 4217.
3. C. J. McHARGUE, *Int. Met. Rev.* **31** (1986) 49.
4. J. T. A. POLLOCK, *Mater. Forum* **9** (1986) 127.
5. G. DEARNALEY, *Thin Solid Films* **107** (1983) 315.
6. J. K. HIRVONEN, *J. Vac. Sci. Technol.* **A3** (1985) 2691.
7. P. J. BURNETT and T. F. PAGE, *J. Mater. Sci.* **19** (1984) 845.
8. C. J. McHARGUE and C. S. YUST, *J. Amer. Ceram. Soc.* **67** (1984) 117.
9. J. K. COCHRAN, K. O. LEGG and G. R. BALDAU, *Proc. Mater. Res. Soc. Symp.* **17** (1982) 549.
10. T. HIOKI, A. ITOH, S. NODA, H. DOI, J. KAWAMOTO and O. KAMIGAITO, *J. Mater. Sci. Lett.* **3** (1984) 1099.
11. C. J. McHARGUE, G. C. FARLOW, C. WHITE, J. M. WILLIAMS, B. R. APPLETON and H. NARAMOTO, *Mater. Sci. Engng* **69** (1985) 123.
12. T. HIOKI, A. ITOH, M. OKHUBO, S. NODA, H. DOI, J. KAWAMOTO and O. KAMIGAITO, *J. Mater. Sci.* **21** (1986) 1321.
13. V. CHINELLATO, V. GOTTARDI, S. LO RUSSO, P. MAZZOLDI, F. NICOLETTI and P. POLATO, *Rad. Eff.* **65** (1982) 31.
14. G. W. ARNOLD, *ibid.* **65** (1982) 17.
15. G. BATTAGLIN, R. DAL MASCHIO, G. DELLA MEA, G. DE MARCHI, M. GUGLIEMI, P. MAZZOLDI and A. PACCAGNELLA, *Nucl. Instrum. Meth.* **B1** (1984) 253.
16. P. MAZZOLDI, in "Glass . . . Current Issues", edited by A. F. Wright and J. Dupuy (Martinus Nijhoff, Doredrecht, 1985) pp. 597–614.
17. M. J. NORGETT, M. T. ROBINSON and I. M. TORRENS, *Nucl. Engng Design* **33** (1975) 50.
18. I. MANNING and G. P. MUELLER, *Comp. Phys. Commun.* **7** (1974) 85.
19. B. R. LAWN and E. R. FULLER Jr, *J. Mater. Sci.* **19** (1984) 4061.
20. G. R. ANSTIS, P. CHANTIKUL, B. R. LAWN and D. B. MARSHALL, *J. Amer. Ceram. Soc.* **64** (1981) 533.
21. *Idem., ibid.* **64** (1981) 539.
22. P. J. BURNETT and T. F. PAGE, *J. Mater. Sci.* **20** (1985) 4624.
23. G. BATTAGLIN, P. MAZZOLDI and R. DAL MASCHIO, in "Induced Defects in Insulators", edited by P. Mazzoldi (Les Editions de Physique, Le Ulis Cedex, 1984) pp. 165–9.
24. G. BATTAGLIN, G. DELLA MEA, G. DE MARCHI, P. MAZZOLDI and A. MIOTELLO, *Nucl. Instrum. Meth.* **B1** (1984) 511.
25. *Idem., ibid.* **B7/8** (1985) 517.
26. G. BATTAGLIN, A. BOSCOLETTO, G. DELLA MEA, G. DE MARCHI, P. MAZZOLDI, A. MIOTELLO and B. TIVERON, *Rad. Eff.* **98** (1986) 101.
27. C. V. McCAUGHAN, R. A. KUSHNER and V. T. MURPHY, *Phys. Rev. Lett.* **30** (1973) 614.
28. B. M. SMETTS and T. P. A. LOMMEN, *J. Amer. Ceram. Soc.* **65** (1982) C80.
29. B. J. BURROW, N. R. ARMSTRONG, R. K. QUINN, B. C. BUNKER, G. W. ARNOLD and D. R. SALMI, *Appl. Surf. Sci.* **20** (1984) 167.

30. E. P. EERNISSE, *J. Appl. Phys.* **45** (1974) 167.
31. G. W. ARNOLD, *Rad. Eff.* **98** (1986) 55.
32. S. S. KISTLER, *J. Amer. Ceram. Soc.* **45** (1962) 59.
33. H. A. SCHAEFFER, in "Strength of Inorganic Glass", edited by C. R. Kurkjian (Plenum Press, New York, 1985) pp. 469–83.
34. J. E. SHELBY, *J. Appl. Phys.* **47** (1976) 4489.
35. S. E. DONNELLY, *Rad. Eff.* **90** (1985) 1.
36. H. H. ANDERSON, J. BOHR, A. JOHANSEN, E. JOHNSON, L. SARHOFF-KRISTENSEN and V. SURFANOV, *Phys. Rev. Lett.* **59** (1987) 1589.
37. A. A. GRIFFITH, *Phil. Trans. Roy. Soc. Lond.* **221A** (1920) 163.
38. P. D. TOWNSEND, J. C. KELLY and N. E. W. HARTLEY, "Ion Implantation, Sputtering and Their Applications" (Academic Press, London, 1976).
39. S. J. BULL and T. F. PAGE, unpublished work (1987).
40. F. P. BOWDEN and D. TABOR, "The Friction and Lubrication of Solids", Part 1 (Clarendon, Oxford, 1958).
41. S. J. BULL and T. F. PAGE, in preparation.
42. J. GODDARD and M. WILLMAN, *Wear* **5** (1965) 114.

Received 5 March
and accepted 1 July 1991